Rubber Chemistry and Technology

Characterisation of Sticky Debris Generated During Smear Wear

--Manuscript Draft--

Manuscript Number:	RCT-D-23-00015R1
Article Type:	Tribute
Keywords:	Rubber Abrasion; Blade Abrasion; Tyre Wear; Smear Wear; Sticky Debris; DQ-NMR
Corresponding Author:	James JC Busfield Queen Mary University of London London, London UNITED KINGDOM
First Author:	Guangchang Wu
Order of Authors:	Guangchang Wu
	Paul Sotta
	Menglong Huang
	Lewis Tunnicliffe
	James JC Busfield
Manuscript Region of Origin:	UNITED KINGDOM
Abstract:	Smear wear behaviour has often been observed during rubber abrasion especially under mild test severities. It generates degraded sticky rubber debris, which often produces erratic measurements of abrasion weight loss. Various practical methods to avoid or remove the debris from the abrasion test surface have been reported, such as applying a drying powder lubricant. However, the detailed mechanism of smear wear behaviour is still not clear. In this paper, various characterisation techniques are applied to investigate the smear wear of both an unfilled NR model compound and a commercial carbon black filled SBR tyre tread compound obtained during blade abrasion testing. The debris showed lower molecular weight and higher oxygen content than the virgin materials. In addition, 75% of the smear wear was found to be de-crosslinked during smear wear, as detected by the DQ-NMR technique. For the first time, it is demonstrated that both the polymer itself and crosslinking points are broken down during smear wear. The effect of the smear layer on friction and abrasion is also discussed.

Characterisation of Sticky Debris Generated During Smear Wear

Guangchang Wu[§], Paul Sotta[†], Menglong Huang[§○], Lewis B Tunnicliffe[§‡], James JC Busfield[§]*

[§]Queen Mary University of London, Mile End Road, London, E1 4NS, United Kingdom

[†]Ingénierie des Matériaux Polymères, Université de Lyon, CNRS, UMR 5223, Université Lyon 1, INSA Lyon, UJM, F-69621 Villeurbanne cedex, France

[‡]Current address: Birla Carbon, 1800 West Oak Commons Court, Marietta, Georgia, 30062, USA

[○]Current address: Continental Reifen Deutschland GmbH, Jaedekamp 30, 30419 Hannover, Germany.

*Corresponding Author: j.busfield@qmul.ac.uk

Abstract

Smear wear behaviour has often been observed during rubber abrasion especially under mild test severities. It generates degraded sticky rubber debris, which often produces erratic measurements of abrasion weight loss. Various practical methods to avoid or remove the debris from the abrasion test surface have been reported, such as applying a drying powder lubricant. However, the detailed mechanism of smear wear behaviour is still not clear. In this paper, various characterisation techniques are applied to investigate the smear wear of both an unfilled NR model compound and a commercial carbon black filled SBR tyre tread compound obtained during blade abrasion testing. The debris showed lower molecular weight and higher oxygen content than the virgin materials. In addition, 75% of the smear wear was found to be de-crosslinked during smear wear, as detected by the DQ-NMR technique. For the first time, it is demonstrated that both the polymer itself and crosslinking points are broken down during smear wear. The effect of the smear layer on friction and abrasion is also discussed.

Keywords: Rubber Abrasion, Blade Abrasion, Tyre Wear, Smear Wear, Sticky Debris, DQ-NMR

Introduction

Abrasion resistance plays an important role for rubber products such as tyres, belts and dynamic seals. Unlike most other engineering materials, rubber materials show very different abrasion mechanisms under different circumstances due to their relative low modulus and unique viscoelastic and frictional properties. Over the past century, a wide range of experimental abraders have been developed to predict abrasion performance and to investigate abrasion mechanisms, such as: needle abrader[1], blade abrader[2,3,4,5,6,7,8,9], Lambourn abrader[10,11,12], DIN abrader[13,14,15], Akron abrader[16,17], LAT 100 abrader[18,19,20,21] and ball on plane abrader[22]. The generally accepted possible mechanisms of rubber abrasion include abrasive wear, fatigue wear and smear wear.

Abrasive wear is the dominant abrasion mechanism when rubber slides against surfaces containing sharp asperities. Stress concentrations generated by the sharp points of contact

cut into the rubber which can then reach the limiting strength of the material and micro-cutting or scratching is observed on the rubber surface [1,23]. Abrasive wear is caused by tensile failure, which normally produces large weight loss. In this case, rubber abrasion is very similar to the abrasion of hard materials such as plastics and metals. When rubber materials slide against smooth rigid abrasives[22] the stress concentrations are much lower, generating a fatigue failure rather than tensile failure to remove wear particles. Therefore, the abrasion of rubber caused by this failure mode is called fatigue wear or adhesion wear. One characteristic of fatigue wear is the formation of a series of periodic parallel ridges perpendicular to the sliding direction, which is known as 'abrasion pattern' or sometimes as 'Schallamach pattern'[24].

Smear Wear

When a rubber compound, and especially a tyre tread compound is abraded under mild conditions, a sticky smear layer is often generated on the rubber surface. This type of abrasion failure is a degradation process which is referred as either smearing or smear wear in the literature. This smear wear, as a distinct class of abrasion mechanism has been reported widely in the literature[11,25,26,27,28,29]. However, only a very limited number of these studies provide a detailed characterisation and discussion of the sticky debris generated by smear wear[30]. It is believed that abrasion failure due to smear wear results from some form of rubber degradation. However, there is no consensus yet on the detailed mechanism responsible for the degradation process[31]. Three potential degradation mechanisms were proposed by Gent and Pulford[28]: 1. thermal decomposition due to local heating; 2. oxidative degradation possibly accelerated by local heating and 3. mechanical rupture of macromolecules to form reactive radical species. Some authors claimed the most plausible mechanism of smear wear formation results from oxidative chain scissions produced by frictional force, in much the same way as occurs during cold mastication of NR[32].

Smear wear can sometimes accelerate[29,33], or for most cases [11,24,34,35,36], decrease the measured wear rate. Such uncertainty brings difficulties in judging the wear rate under laboratory testing conditions. Thus, a lot of effort has been made to avoid the formation of the smear layer or simply to remove it from the wear surface[36]. The most common ways encountered in standard tests include feeding a drying powder into the nip between the rubber and the counterpart surface, testing using an inert atmosphere, or by lowering the ambient test temperature. The effect of various drying powders such as magnesium oxide, Fuller's earth and French chalk on abrasion have all been investigated[27]. The use of magnesia appears to be the most effective way to prevent the generation of smear wear. However, there may be two competing effects of feeding powder. The first effect results in the abrasion rate being increased as the powder helps removal of the lubricating low molecular weight impurities from the rubber surface. In contrast, the abrasion loss could also be reduced because the powder acts as a lubricant between the rubber and the track.

To understand oxidative deterioration mechanisms, many wear tests were performed under different atmospheric conditions. Schallamach[24] investigated the abrasion of NR in an inert atmosphere. Following a first abrasion step in nitrogen, switching the atmosphere to air resulted in a drop of the abrasion rate due to an instantaneous formation of a smear layer.

The abrasion rate then increased with time and was finally greater than the steady state rate of abrasion in nitrogen. When the abrasion rate of a rubber was low in air due to smear wear, the subsequent abrasion in nitrogen was often greater than in air. If smear debris was obviated by the use of a suitable powder, the abrasion was greater in air than in nitrogen. However, other researchers demonstrated that some rubbers like NR and SBR only degraded in the presence of oxygen. The rate was much less when they were abrasion tested in an inert atmosphere such as nitrogen. BR produced only dry debris during abrasion[28]. It was proposed that any free radicals produced by main chain scission in a BR compound could rapidly react with the polymer itself, resulting in an increase in crosslinking density rather than degradation.

Temperature also has significant influence on rubber abrasion. Not only does it affect the viscoelastic properties of rubber itself, but it can also determine the actual abrasion mechanism. Different abrasion mechanisms dominate within different temperature ranges. At lower temperatures, abrasive wear dominates, while moderate temperatures produce fatigue wear, and higher temperatures produce smear wear. As a result, the wear mechanism can be switched from one mechanism to another, or the contributions between different mechanisms will be completely redistributed. Muhr and Roberts[35] demonstrated that the smear wear mechanism plays a more important role at higher temperatures. They used an Akron type abrader running on a smooth glass slide. The results showed that both smeared and rubber particles were deposited on the glass. In the temperature range from -30 to 60 °C, the higher ambient temperature resulted in a greater production of smear wear, and at lower temperature there was a greater number of debris particles. In the case of temperatures below -20 °C no smear debris was present.

Although smear wear has been investigated using various techniques, there has been only a very limited number of systematic studies undertaken on the characterisation of the smear wear. Therefore, some fundamental questions remain open, such as: What is the smear layer comprised of? How does it affect the abrasion and friction behaviour? This paper attempts to address these questions. Various techniques were used to characterise the smear wear with respect of their glass transition temperature, chemical composition, molecular weight, and crosslinking density.

Experimental Section

Materials

Both an unfilled model compound and a commercial passenger tyre tread compound were used in this study. The model compound was a sulphur crosslinked, unfilled natural rubber (NR0) which was mixed on an open two-roll mill. The tread compound was a styrene-butadiene rubber filled by 50 phr N234 (SBR50) supplied by Cabot Corporation, MA, USA. The tread compound, SBR50 was mixed in a Banbury-type internal mixer with a chamber volume of 1 L. The optimal curing conditions were determined using an Alpha 2000 rheometer. The detailed formulations and curing conditions are given in Table 1.

Blade Abrasion

The abrasion tests were conducted using a blade abrader, which was originally designed and developed by Champ et al[3]. The apparatus for blade abrasion testing is shown in Figure 1. The blade had an initial wedge shape when manufactured but as it was used extensively it also experienced significant wear. Therefore, the blade tip reached an equilibrium state which was used throughout experiments with an approximately constant sharpness of 0.3 mm radius. It was fixed at one end of a freely pivoted arm. The whole arm was mounted on a spring cantilever, whose horizontal displacement was measured by a non-contact displacement sensor. The displacement sensor was calibrated to obtain the relationship between the horizontal force applied on the blade and the output voltage measured by Agilent 34401 multimeter. The other side of the arm was attached to a simple dashpot damper to reduce the vibration, resulting from the sliding of the blade over the sample, to a typical value of about 0.5mm.

Rubber wheel test specimens with an internal diameter of 12.5 mm, an external diameter of 68 mm and having a thickness of 12.5 mm were compression moulded using a hot press to the optimal curing conditions as shown in Table 1. The cured rubber wheel was fixed on a shaft, which was driven by an induction motor through a gearbox. It was rotated against a stationary blade at 21 rpm, which corresponded to an average sliding velocity of 70 mm/s. A dead weight positioned on the top of the blade was used to apply the designated normal force. The sample weight was measured, and the wear debris was collected for the further analysis after a certain testing period. The material weight loss rate here is defined as: $\dot{m} = \mathrm{d}m/\mathrm{d}n$, where m is the material weight and n is the number of sample rotation cycles, or wear cycles.

Differential Scanning Calorimetry (DSC)

DSC was conducted to measure the glass transition temperature for both the smear wear and unabraded bulk materials. Calorimetry measurements were made using a TA Q2000. Samples of 5 to 10 mg were placed in aluminium crucibles for testing. Samples were cooled to -80 °C and heated up to 20 °C at a rate of 2 °C/min under a flushing nitrogen atmosphere.

TGA

TGA performed on TA Q500 was used to characterise the chemical content, thermal stability and amount of degraded rubber of the smear wear. Both air and nitrogen atmospheres were used. The samples were first heated up from room temperature to 700 °C at 20 °C/min in a nitrogen atmosphere. Following this, the atmosphere was changed to air and the temperature was further increased from 700 °C to 1000 °C at 50 °C/min. An alternative test was also used on a different sample using an air atmosphere throughout from room temperature to 1000 °C at 20 °C/min.

Energy-dispersive X-ray Spectroscopy (EDX)

The SEM-EDX analyses were performed on an FEI Inspect Scanning Electron Microscope (SEM) equipped with an EDX-detector. For NR0, the specimen was coated with carbon to make it conductive. As SBR50 is above the filler network percolation threshold, the samples were conductive and no conductive coating was required. The analyses were performed at a 10 kV accelerating voltage and a beam current in the range of 1 to 3 nA for up to 60 seconds.

Gel Permeation Chromatography (GPC)

The molecular weights of the smear wear and rubber melts before vulcanisation were determined using GPC. The smear wear and rubber melt were dissolved in Tetrahydrofuran (THF) with 2% Triethylamine (TEA). A filter with 0.1 µm pore size was used to filter the solution. After filtration the solutions were used to conduct the GPC on an Agilent 1260 infinity system equipped with Refractive Index Detector (RID) and variable wavelength detector, 2 PLgel 5 µm mixed-C columns (300×7.5mm), a PLgel 5 mm guard column (50x7.5mm) and an autosampler. The columns and the RID were operated at 40 °C. The instrument was calibrated with linear narrow poly(methyl methacrylate) standards in range of 550 to 2136000 g/mol.

Bound Rubber Measurement

Bound rubber testing was performed on the aged smear wear of the tread compound to measure how much rubber remained insoluble in the smear wear. Test samples of around 20 mg were immersed in 20 ml toluene for 120 hours. The solvent was renewed after 48 hours. After extraction the samples were dried for 24 hours in air at room temperature and then for 24 hours in an oven at 100 °C. The percentage of the bound rubber, R_b, was then calculated according to the following equation:

$$R_b\% = \frac{m_d - m_o \times f_f}{m_o \times f_p} \qquad \text{(Equation 1)}$$

where m_d is the dry mass after extraction, m_o is the mass of the original specimen, f_f and f_p are the filler and polymer fractions according to the compound's original formulation.

DQ-NMR

Time-domain proton NMR spectroscopy is based on the measurement of the residual tensorial interactions, which originate from incomplete motional averaging of chain segments fluctuating rapidly between topological constraints, such as crosslinks or chain entanglements[37,38]. The local anisotropy of reorientational motions is described by a nonzero dynamical orientation of the polymer backbone $\langle P_2(\cos\theta)\rangle$ defined as the time average of the second-order Legendre polynomial[39]:

$$\langle P_2(\cos\theta)\rangle = \frac{1}{t}\int_0^t \left(\frac{3\cos^2\theta(t\prime)-1}{2}\right) \mathrm{d}t' \qquad \text{(Equation 2)}$$

in which θ is the time-dependent angle between the local chain direction (segmental orientation) and a reference direction. At high enough temperature (with respect to *Tg*), reorientational motions are fast and the above time average stabilizes rapidly at short times *t*. For a network chain, topological constraints such as entanglements and cross-links lead to

a nonzero permanent time average, which gives a dynamic average orientation of the polymer backbone, related to the length R and orientation α of the end-to-end vector. In a freely jointed rigid rod chain model, the average segment orientation is

$$\langle P_2(\cos\theta)\rangle \approx \frac{3}{5}\frac{R^2}{N^2b^2}\frac{3\cos^2\alpha-1}{2} \approx S_b\frac{3\cos^2\alpha-1}{2} \quad \text{(Equation 3)}$$

where N is the number of statistical segments (freely jointed rigid rods) between constraints and b the statistical segment length.

The overall NMR signal is then the sum of contributions from all chains. From this, an average value of the local backbone orientation with respect to the end-to-end vector arises, which corresponds to S_b (see eq 4). Using the usual result for ideal chains $R^2 \approx \mathrm{N}b^2$, it may be written

$$S_b \approx \frac{3}{5}\frac{R^2}{N^2b^2} \approx \frac{1}{N} \approx \frac{1}{M_c} \approx \nu \quad \text{(Equation 4)}$$

Since the proton dipolar coupling, which is NMR observable, depends on molecular orientation, the nonzero dynamic orientation of the polymer backbone S_b is detected in NMR because it gives a nonzero residual dipolar coupling. S_b is calculated from the experimentally measured average residual dipolar coupling constant D_{res}, by comparison with its static counterpart, D_{static}, as (k is a correction factor <1 accounting for the spin arrangement and motions within a statistical segment)

$$S_b = k\frac{D_{res}}{D_{static}} \quad \text{(Equation 5)}$$

According to eqs (4) and (5), D_res is inversely proportional to the average molecular weight of network chains between cross-links M_c or, equivalently, proportional to the cross-link density ν. Entanglements also contribute to the NMR signal. Assuming a constant entanglement density and additivity of entanglement and cross-link densities, we may write $D_{res} \propto 1/M_c + 1/M_e$, with M_e the entanglement molecular weight.

Two sets of data, the Double Quantum build-up (I_{DQ}) and a reference decay (I_{Ref}), are collected in each test. While all protons in the material contribute to I_{Ref}, only those with a non-zero D_{res} value, which are those belonging to elastically active chains, contribute to I_{DQ}. The amount of defects (dangling chains, loops, sol chains and oligomers) can be estimated and their contribution have to be subtracted from I_{Ref} prior to computing the normalized I_{DQ}.

For time-domain proton NMR measurement, the sticky wear debris of NR0 and uncured NR0 melt were put into a test tube and inserted as solid samples into the measuring probe. Experiments were carried out on a Bruker Minispec mq20 proton low-field NMR spectrometer operating at 0.5 Tesla with 90° pulses of 2 µs and a dead time of 12 µs. The experiments were done at 60 °C (that is about *T*g + 120°C) to ensure fast motions and proper time averaging of spin interactions.

Results and Discussion

Abrasion Behaviour

The blade abrasion process is typically divided into two stages: initiation state and steady state. In the initiation state, the material weight loss rate, $\dot{m}$, increases as the number of wear cycles increases, while in the steady state it is constant. The cumulative weight loss during blade abrasion test under a 20 N normal force for NR0 is shown in Figure 2, which clearly highlight these two different wear states.

The sample surface showed very different phenomena during these different wear stages. A smear layer was observed on the sample surface at the beginning of the wear test for both NR0 and SBR50. An example is shown in Figure 3. On the other hand, an abrasion pattern was formed on the rubber surface as shown in Figure 4. Such an abrasion pattern slowly developed during the initiation state until an established geometry was developed when approaching the steady state. Figure 5 shows the abrasion surface developed for SBR50 during these different wear stages, which demonstrates the transition from the sticky surface to an abrasion pattern.

However, it was not necessary to have a fully developed abrasion pattern to achieve a constant material weight loss rate, $\dot{m}$. The development of the wear pattern was highly dependent on the test conditions. Generally, a higher normal force helped the pattern to develop. For example, when the normal force was reduced to 4 N for NR0 and 12N for SBR50, no abrasion pattern was observed, but the smear wear was always observed during the initiation stage. Figure 6 (a) and (b) show collected sticky wear debris from NR0 and SBR50 that have been abraded under different conditions. Compared to fatigue wear, smear wear can be initiated under much lower loading severities. More importantly, it seems that that smear wear can exist independently of other wear mechanisms during wear testing.

Glass Transition Temperature of Smear Wear

The DSC trace of sample NR0 is shown in Figure 7. The glass transition temperature is defined as the intercept of two lines as shown in the figure at the onset of the *C*p jump). There is no significant difference in the DSC traces between the bulk material and smear wear. The glass transition temperatures of the bulk and of the debris were similar, at approximately -65 °C for NR0. There is no change of *T*g for SBR50 either. The glass transition temperature was around -30 °C (result not shown). There was no significant change of the local relaxation of the rubber chains, although the molecular weight for the smear wear was reduced dramatically, as shown by the independent GPC measurements.

Thermal and Thermo-oxidative Degradation of the Smear Wear

Figure 8 shows the TGA weight loss curves in nitrogen up to 700 °C and in air from 700 °C to 1000 °C for NR0 and SBR50. All volatile components and polymer material were degraded in nitrogen below about 500 °C. Then the remaining carbon-based fillers were combusted in air above 700 °C. The TGA curve of the smear wear performed in this way is very similar to that of bulk material. The smear wear consisted of the same amount of filler as the bulk material.

However, the thermal stability of the smear wear was inferior, since it decomposed at a faster rate in the nitrogen atmosphere. This probably results from a lower molecular weight of the smear wear, since it is known that an increase in molecular weight increases thermal stability[40].

TGA was also performed in air atmosphere over the entire temperature range. The results are shown in Figure 9. Under this thermo-oxidative conditions, three steps were clearly identified for the rubber decomposition. For NR0 the volatile low molecular weight materials degraded first below 320 °C. Following this, the polymer itself started to degrade. The last step was the degradation process of the char formed during the second step. For SBR50, the volatile species degraded first below 420 °C. Then the polymer decomposed below 500 °C. Finally, the carbon black filler and the char formed by polymer degradation during the second step degraded at the highest temperature[41].

Compared with the unworn bulk material, the smear wear has a broadly similar degradation curve. However, the thermal stability of the smear wear was inferior since they decompose at a faster rate. The smear wear seems to contain a higher volatile content and a lower rubber content. There is a greater charring effect for the smear wear being degraded in the air. The blooming effect during abrasion is one possible reason for the larger volatile content. Large stress and high temperature build-up on the abraded surface help the volatile species to migrate to the rubber surface[42]. In addition, the rubber degradation due to the smear wear could also break down the high molecular weight materials into lower molecular weight components. The lower rubber content in the smear wear indicates that rubber molecules are degraded, at least partly, during the smear wear. The larger char amount probably results from more free radicals in the smear wear which possibly promotes the char formation via thermal oxidation[41]. These free radicals probably come from the breakdown of the large polymer chains into small fragments. The weight percentage loss of each step for thermal oxidative degradation is shown in Table 2 and Table 3 for NR0 and SBR50, respectively.

Molecular Weight and Oxygen Content of the Smear Wear

The smear wear has an oily, liquid like apparent behaviour, which implies it has a lower molecular weight. The smear wear generated during abrasion was immediately dissolved in THF to measure the molecular weight using GPC. The results were compared with the original molecular weight of the uncured rubber melts extracted in THF as shown in Figure 10. First of all, a signal response was detected for the smear wear, which means the debris were, at least partly, soluble. Secondly, the GPC trace for the debris shifted to the right compared to the rubber melt, which confirmed that there was a longer retention time suggesting that smaller rubber molecules were present in the smear wear. There were two peaks for the GPC traces of SBR50 melts, which was probably due to a non-uniform distribution of the molecular weight. Once being abraded, the molecular weight of the smear wear became smaller and more uniformly distributed.

The weight average molecular weight, Mw, the number average molecular weight Mn and the polydispersity, PD are shown in Table 4. The average molecular weight of the smear wear was an order of magnitude lower than that of the original rubber melts. The rubber molecules are clearly being broken into small fragments during smear wear, which results in this sticky liquid like debris being produced with a reduced molecular weight. Since the debris are soluble, it can also confirm that there is a decrosslinking process operating during smear wear. The sulphur-sulphur crosslinking points are weaker than the carbon-carbon polymer backbone, and they are probably preferentially broken during abrasion. As a consequence, the breakdown of both the crosslinking points and the polymer backbone results in the three-dimensional crosslinked network being degraded into small soluble fragments.

The oxidative deterioration could be one of the reasons for the breakdown of polymer chains during the smear wear. In order to verify this, a simple elemental mapping was undertaken using EDX to determine the oxygen content in the smear wear. The results are shown in Table 5. For NR0 carbon element was eliminated in the analysis since the sample was carbon coated. The smear wear had more oxygen content compared to the bulk materials - especially for SBR50. This supports an oxidative degradation mechanism during the formation of smear wear. In addition, the sulphur content was lower in the smear wear.

Changing of Solubility of the Smear Wear

One interesting phenomenon was observed for the filled rubber, after leaving the smear wear exposed to the atmosphere for a time period in excess of 24 hours. Figure 11 a) shows the fresh smear wear of SBR50 in toluene. The debris appeared to be completely soluble in the solvent. The undissolved carbon black formed a suspension, which resulted in the solution becoming completely black. It was confirmed by GPC that the rubber molecular chains were broken into smaller pieces or fragments due to the large shear force encountered during the abrasion. Conversely, the average molecular weight measured in the smear wear remained quite high compared to the average molecular weight between crosslinks in the rubbers, which is less than 100 monomers for about 1.5 phr sulfur. Thus, the fact that fresh smear wear can be dissolved in toluene potentially confirms that some degree of devulcanization occurred.

Figure 11 b) shows the aged smear wear in the same solvent. Large insoluble debris are clearly visible at the bottom. The solution remains transparent. It is thus apparent that the solubility of the smear wear was significantly reduced with the dwell time. The change of the solubility of the smear wear could be ascribed in principle to two mechanisms. The first one is that the broken crosslinks can somehow recover and reform a 3-D polymer network. However, this seems to be unlikely since sulphur vulcanisation requires thermal energy to be activated and the sulphur content in the smear wear is apparently reduced as evidenced by EDX characterisation. Another mechanism is that potentially the oxidation process introduces some form of cross-linking network. Another possible mechanism might be that the filler network in the smear wear can recover with time in a similar manner to the flocculation process during melt processing and the polymer chain fragments can easily be reabsorbed onto the filler surface forming “bound rubber”[43,34]. During the abrasion process, the fracture of either polymer backbone or crosslinks results in the formation of free radicals. The filler particles and the anti-oxidant can both act as strong radical scavengers. For the filler particles this is due to their high surface energy and presence of stable spin-unpaired electrons[44,45], which can trap free radicals and stabilise them. Therefore, the solubility of the aged smear wear decreases. The amount of the insoluble rubber in the aged smear wear was determined using the same technique used to measure the bound rubber content of an unvulcanised rubber melt. The insoluble rubber for aged smear wear and rubber melt for SBR50 were 57 % and 41%, respectively. Thus, the amount of insoluble rubber of the aged smear wear was larger than the bound rubber of the uncured rubber melt, supporting the idea that some form of crosslinked network was formed.

Crosslinking Network of the Smear Wear

It would also be useful to measure to what extent the rubber was de-crosslinked and the residual crosslinking network of the smear wear. However, due to the unique feature of the smear wear (irregular shape, limited amount and liquid like morphology) the conventional crosslinking density measurements (swelling test and mechanical testing) were impractical. Proton DQ-NMR is an appropriate technique for the study of structural constraints in rubber

materials. In this work only NR0 and SBR80 (a similar formulation as SBR50, with a higher value of 80 phr CB) were tested, as it was generally quite difficult to collect enough wear debris. The test results are shown in Figure 12 for NR0. The results involve two sets of experimental data, the DQ buildup (I_{DQ}) and a reference decay (I_{ref}). In both cases, the sticky wear debris clearly has a different NMR response compared to the uncured rubber melt (in the case of NR0) and compared to the unworn sample (in the case of SBR80). The DQ signal is smaller and badly shaped, which indicates that wear debris behave as if only a fraction remains crosslinked, and a majority fraction of the smear wear has been de-crosslinked.

For quantitative analysis, the function $f(t) = I_{ref}(t) - I_{DQ}(t)$ is plotted in Figure 13, for both the uncured NR melt and for the NR0 smear wear. This function is used to fit and subtract the long-time tail of I_{ref}, which corresponds to uncrosslinked network defects (dangling chains, loops and sol chains). The curves are extremely different in each case. The contribution corresponding to the long-time tail is shown in the graph as well. While the defect fraction in the rubber melt is about 7.6% of the total signal (which is a typical value in such materials), this fraction in the smear wear is about 75% of the total. This would mean that in the debris about 75% of the material is composed of uncrosslinked polymer. The smear wear has much smaller molecules having an order of magnitude lower molecular weight, which is correlated to a much larger amount of uncrosslinked defects (one order of magnitude higher). The ref and DQ signals for the SBR80 sample are shown in Figure 14. For SBR80, the defect fraction in the unworn sample is about 27% and reaches about 55 ± 4% in the debris. The crosslinking density of the remained crosslinked network can be obtained independently of relaxation effects by normalising I_{DQ} by the total signal after subtraction of the defect contribution (I_{def}), which can be expressed as $I_{nDQ} = I_{DQ} / (I_{DQ} + I_{ref} - I_{def})$. The result is shown in Figure 15 for the NR samples and in Figure 16 for the SBR80 samples. The I_{nDQ} signal tends to a plateau at 0.5, which indicates that the defect fraction was correctly estimated. The initial slope of I_{nDQ} gives access to D_{res}. For NR samples, the signal from the crosslinked part of the debris (25%) has a larger initial slope, meaning it is more crosslinked than the uncured rubber melt. It is possible that the collected smear wear contains a small proportion of mechanically fractured rubber particles, which have similar crosslinking densities to the unworn cured rubber. For the SBR80 sample, the crosslinked part of the debris (about 55%) has a crosslink density similar to that of the unworn sample. Note that an additional unworn SBR80 sample, manually cut into sub-millimeter size fragments, was measured. It was found that it gave similar results as the bulk unworn SBR80 sample, which shows that the difference between unworn SBR80 and its debris is effectively due to smear wear and not only to some mechanical fragmentation process.

Effect of the Smear Layer on Rubber Friction and Abrasion

Figure 17 shows the frictional behaviour of SBR50 during abrasion. The frictional force increases gradually as the abrasion starts. It reaches an equilibrium plateau after about 1000 cycles. The initial increase of the friction force is counter-intuitive from a viscoelastic perspective since, as the temperature increases, the friction force contribution from viscoelasticity should decrease. This rise in frictional force is ascribed to the formation of the smear layer on the surface. The increase of the friction as the smear layer is developed is probably due to two effects. On the one hand, as the smear layer is essentially a viscous lower

molecular weight liquid polymer, the low modulus of the smear layer present on the rubber surface could give a larger real contact area between the rubber surface and the counterpart. On the other hand, the devulcanization processes as discussed above may make the abraded surface more viscous. Therefore, both the adhesive and viscous contributions to the frictional forces might be increased as the smear layer is developed[46].

When the wear test is halted and the smear layer present on the rubber surface is allowed to age in air as described previously, then upon recommencing the wear test, it becomes much easier to abrade the bulk rubber wheel. Figure 18 shows the blade abrasion loss for SBR50 at a 26 N normal force. The mass was measured every 500 revolutions until the end of each day. Then the test was stopped, and the sample was left in the lab overnight prior to recommencing abrasion testing the next day. Each jump in the weight loss resulted from the very first measurement taken at the start of each day after just 500 additional revolutions. Clearly, leaving the sample overnight allowed the smear layer to age, as already discussed in Section 'Changing the solubility of the Smear Wear'. This ageing clearly resulted in a faster rate of abrasion loss for the first few revolutions. Then as the new smear layer developed, the rate of abrasion loss was reduced.

Conclusion

This paper presents a systematic study on characterisation of the sticky debris generated during smear wear. The smear wear was achieved using blade abrasion under low test severities (low normal force) and the smear debris was collected. Due to the local temperature increase and input mechanical energy, both rubber chains and crosslinks can break down during abrasion to form smear wear. The smear wear is a form of degraded rubber, which has a greater volatile content and more oxygen content according to EDX measurements. This confirms the thermo-oxidative effect during smear wear.

Although there is no significant change of the glass transition temperature, the molecular weight of this smear wear is almost an order magnitude lower than that of the original rubber, which gives it a sticky and liquid like morphology. The degraded rubber chain fragments and broken filler network in the smear layer can recover with ageing time, at least in part. As a consequence, the solubility of the smear wear in solvent decreases with time.

In addition, a decrosslinking effect is confirmed qualitatively and quantitatively using DQ-NMR. In NR, around 75% of the smear wear is composed of un-crosslinked network defects, while this fraction is about 55% in CB-filled SBR. It is believed that during smear wear the three-dimensional rubber network is thermo-mechanically broken down into small fragments. It is conjectured that, in addition to this fragmentation process, the smear wear material experiences severe fatigue degradation which forms this lower molecular weight and de-crosslinked smear wear.

The initial formation of the smear layer on rubber surface during abrasion increases the friction force since the smear layer has both a lower modulus and a higher viscosity. These effects enhance both the adhesive and viscous contributions of the rubber friction. The old smear layer with lower solubility can be easily abraded off, which leads to a higher rate of abrasion loss.

Acknowledgements

The authors would like to thank Prof Alan Thomas, who motivated us to undertake the investigation. This was one of the last projects he was an active participant from inception to results evaluation and all the QMUL team will be forever indebted for his wonderful insights in completing this and many other investigations into the behaviour of rubber. We would also like to thank Evangelos Koliolios for helping to proofread the manuscript. Dr. Guangchang Wu would like to thank Cabot and the Soft Matter Group at Queen Mary University of London for doctoral funding that supported this investigation.

References

[1] A. Schallamach, Abrasion of rubber by a needle. Journal of Polymer Science, 1952. 9(5): p. 385-404.
[2] A.H. Muhr and S.C. Richards, ABRASION OF RUBBER BY MODEL ASPERITIES. Kautschuk Gummi Kunststoffe, 1992. 45(5): p. 376-379.
[3] D. Champ, E. Southern, and A. Thomas, Fracture mechanics applied to rubber abrasion, in Advances in Polymer Friction and Wear. 1974, Springer. p. 133-144.
[4] E. Southern and A.G. Thomas, Studies of rubber abrasion. Rubber chemistry and technology, 1978. 52(5): p. 1008-1018.
[5] G. Wu, A.G. Thomas, and J. Busfield, Effect of the blade sharpness on the blade abrasion of rubber. Constitutive Models for Rubber VIII, 2013: p. 65.
[6] G.C. Wu, A. Mukaiyama, A.G. Thomas, and J.J.C. Busfield, Estimating strain energy release rate during blade abrasion at steady state using finite element analysis. Constitutive Models for Rubber IX, 2015: p. 119.
[7] Y. Fukahori, H. Liang, and J.J.C. Busfield, Criteria for crack initiation during rubber abrasion. Wear, 2008. 265(3-4): p. 387-395.
[8] H. Liang, Y. Fukahori, A.G. Thomas and J.J.C. Busfield, Rubber abrasion at steady state. Wear, 2009. 266(1-2): p. 288-296.
[9] H. Liang, Y. Fukahori, A.G. Thomas and J.J.C. Busfield, The steady state abrasion of rubber: Why are the weakest rubber compounds so good in abrasion? Wear, 2010. 268(5-6): p. 756-762.
[10] J. Adams, J. A. Reynolds; W. E. Messer; L. H. Howland, Abrasion Resistance of GR-S Vulcanizates. Rubber Chemistry and Technology, 1952. 25(2): p. 191-208.
[11] L. Howland, W. White, and W. Messer, The Effect of Masterbatching, Compounding, and Testing Variables on Constant-Slip Abrasion Results. Rubber Chemistry and Technology, 1954. 27(4): p. 977-995.
[12] R. Ramakrishnan, J.A. Donovan, and A.I. Medalia, The effect of abrading surfaces on the wear of rubber tread compounds. Rubber Chemistry and Technology, 1995. 68(4): p. 609-622.
[13] N. Mathew, and S. De, Scanning electron microscopy studies in abrasion of NR/BR blends under different test conditions. Journal of Materials Science, 1983. 18(2): p. 515-524.
[14] Y.S. Kim, H.S. Byun, S. Kim, W.Y. Kim, S.C. Han and A.G. Gent , Abrasion of selected rubber compounds with a DIN abrader. Korea Polymer Journal, 1999. 7(2): p. 116-123.
[15] K. Pal, T. Das, R. Rajasekar, S.K. Pal and C.K. Das, Wear characteristics of styrene butadiene rubber/natural rubber blends with varying carbon blacks by DIN abrader and mining rock surfaces. Journal of applied polymer science, 2009. 111(1): p. 348-357.
[16] A. Schallamach, The role of hysteresis in tire wear and laboratory abrasion. Rubber Chemistry and Technology, 1960. 33(3): p. 857-867.
[17] Z. Wei, Y. Lu, Y. Meng and L. Zhang, Study on wear, cutting and chipping behaviors of hydrogenated nitrile butadiene rubber reinforced by carbon black and in-situ prepared zinc dimethacrylate. Journal of Applied Polymer Science, 2012. 124(6): p. 4564-4571.
[18] K. Grosch, Correlation between road wear of tires and computer road wear simulation using laboratory abrasion data. Rubber chemistry and technology, 2004. 77(5): p. 791-814.
[19] M. Heinz and K.A. Grosch, A laboratory method to comprehensively evaluate abrasion, traction and rolling resistance of tire tread compounds. Rubber Chemistry and Technology, 2007. 80(4): p. 580-607.
[20] K. Grosch, Rubber abrasion and tire wear. Rubber Chemistry and Technology, 2008. 81(3): p. 470-505.

[21] V. Dorozhkin, A study of the combined use of carbon black and silicon dioxide in tyre tread formulations. Part 3. Laboratory service tests of tread rubbers. International Polymer Science and Technology, 2015. 42(5): p. T35.
[22] Z. Mané, J.-L. Loubet, C. Guerret, L. Guy, O. Sanseau, L. Odoni, L. Vanel, D.R. Long and P. Sotta, A new rotary tribometer to study the wear of reinforced rubber materials. Wear, 2013. 306(1): p. 149-160.
[23] A. Schallamach, Friction and abrasion of rubber. Rubber Chemistry and Technology, 1958. 31(5): p. 982-1014.
[24] A. Schallamach, Abrasion, fatigue, and smearing of rubber. Journal of Applied Polymer Science, 1968. 12(2): p. 281-293.
[25] S. Nakano, Y. Yamahashi, F. Kaneko, T. Zushi, T. Mabuchi, T. Kawamura, and T. Tada. Effect of molecular structure on the mechanochemical wear behavior of hydrogenated and conventional sbr rubbers. KGK Kautschuk Gummi Kunststoffe, 2021. 74:p. 56–61.
[26] A. Rudakov, and E. Kuvshinskii, The mechanism of abrasion of vulcanized rubber. Rubber Chemistry and Technology, 1964. 37(1): p. 291-296.
[27] K. Grosch, and A. Schallamach, Relation between abrasion and strength of rubber. Rubber Chemistry and Technology, 1966. 39(2): p. 287-305.
[28] A.N. Gent, and C.T.R. Pulford, Mechanisms of rubber abrasion. Journal of Applied Polymer Science, 1983. 28(3): p. 943-960.
[29] Y. Uchiyama, The effect of environment on the friction and wear of rubber. Wear, 1986. 110(3-4): p. 369-378.
[30] G. Wu, PhD thesis: The mechanisms of rubber abrasion. 2017, Queen Mary University of London.
[31] S.W. Zhang, Advances in the Studies on Rubber Abrasion. Tribology International, 1989. 22(2): p. 143-148.
[32] W. Arayapranee, Rubber abrasion resistance. Abrasion Resistance of Materials, InTech, Rijeka, 2012: p. 147-166.
[33] S. Gehman, C. Wilkinson Jr, and R. Daniels, Smearing of Vulcanized Rubber. Rubber Chemistry and Technology, 1955. 28(2): p. 508-518.
[34] V. Garten, K. Eppinger, and D. Weiss, Studies on Abrasion and Wear of Rubber. I. The Chemistry of Carbon Black and Its Effect on Abrasion as Determined by the National Bureau of Standards Method. Rubber Chemistry and Technology, 1956. 29(4): p. 1434-1444.
[35] A.H. Muhr and A.D. Roberts, Rubber Abrasion and Wear. Wear, 1992. 158(1-2): p. 213-228.
[36] M. Huang, M. Guibert, J. Thévenet, C. Fayolle, T. Chaussée, L. Guy, L. Vanel, J.-L. Loubet and P. Sotta, A new test method to simulate low-severity wear conditions experienced by rubber tire materials. 2018. 410: p. 72-82.
[37] A. Vieyres, R.P. Aparicio, P.-A. Albouy, O. Sanseau, K. Saalwächter, D.R. Long and P. Sotta, Sulfur-Cured Natural Rubber Elastomer Networks: Correlating Cross-Link Density, Chain Orientation, and Mechanical Response by Combined Techniques. Macromolecules, 2013. 46(3): p. 889-899.
[38] K. Saalwachter, Proton multiple-quantum NMR for the study of chain dynamics and structural constraints in polymeric soft materials. Progress in Nuclear Magnetic Resonance Spectroscopy, 2007. 51(1): p. 1-35.
[39] G. Mitchell, A wide-angle X-ray study of the development of molecular orientation in crosslinked natural rubber. Polymer, 1984. 25(11): p. 1562-1572.
[40] J. Hacaloglu, T. Ersen, N. Ertugrul, M.M. Fares and S. Suzer Pyrolysis mass spectrometric analysis of styrene-butadiene block and random copolymers. European Polymer Journal, 1997. 33(2): p. 199-203.
[41] S. Bourbigot, J.W. Gilman, and C.A. Wilkie, Kinetic analysis of the thermal degradation of polystyrene–montmorillonite nanocomposite. Polymer Degradation and Stability, 2004. 84(3): p. 483-492.
[42] S.H. Nah and A.G. Thomas, Migration and blooming of waxes to the surface of rubber vulcanizates. Rubber Chemistry and Technology, 1981. 54(2): p. 255-265.
[43] L.B. Tunnicliffe, Thixotropic flocculation effects in carbon black reinforced rubber: Kinetics and thermal activation. Rubber Chemistry and Technology, 2021. 94: p. 298–323.
[44] G. Kraus and R.L. Collins, Odd Electrons in Rubber Reinforcing Carbon Blacks. Rubber Chemistry and Technology, (1959) 32: p. 107-117
[45] R.L. Collins, M.B. Bell and G. Kraus, Unpaired Electrons in Carbon Blacks. Rubber Chemistry and Technology, (1960) 33: p. 993-1004
[46] A. Tiwari, N. Miyashita and B. N. J. Persson, Rubber Wear and the Role of Transfer Films on Rubber Friction on Hard Rough Substrate, Tribology Letters, 2021. 69: p. 42

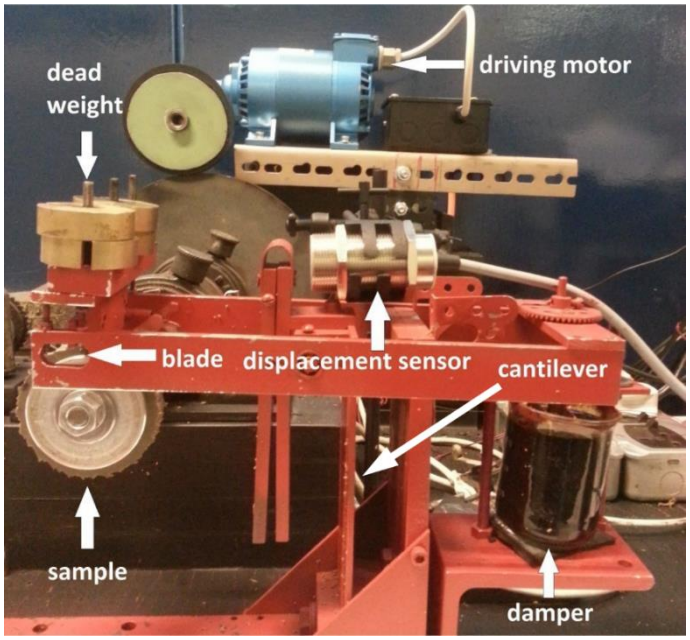

Figure **Error! Main Document Only.**. Blade abrasion apparatus.

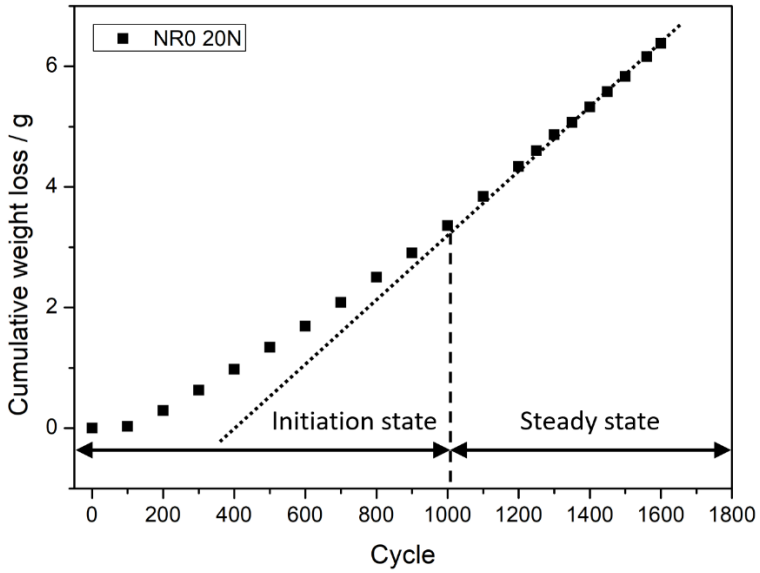

Figure **Error! Main Document Only.**. *Cumulative weight loss at 20 N normal force.*

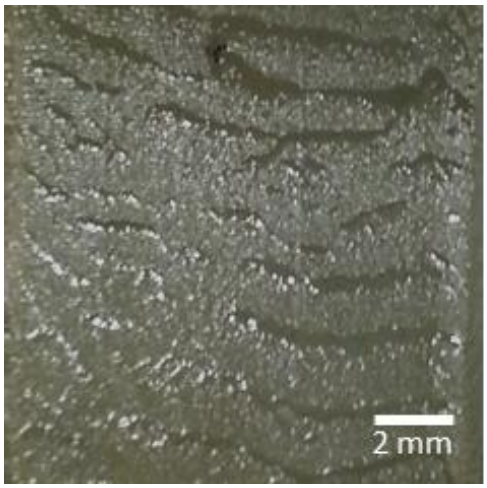

*Figure **Error! Main Document Only.**.Smeared rubber surface of NR0 tested under a normal force of 4N after 1000 wear cycles.*

*Figure **Error! Main Document Only.**. The fully developed abrasion pattern under 8 N, 12 N, 16 N and 20 N normal force from left to right for NR0.*

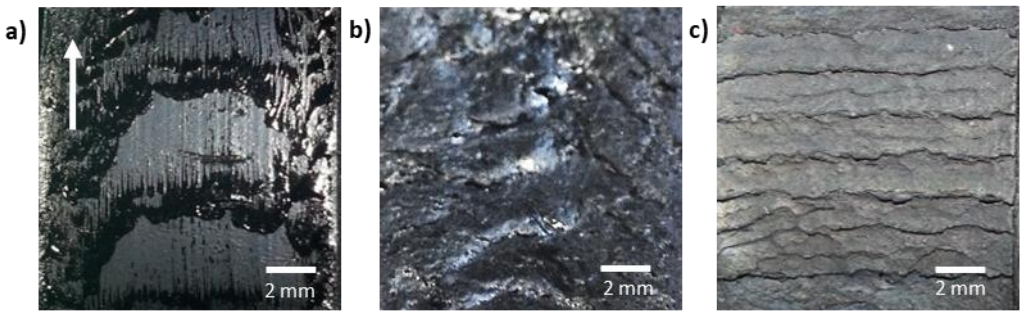

Figure 5. Abrasion surface of SBR50 under 20N normal force: a) smear layer surface at 10000 cycles, b) transition phase surface at 60000 cycles, c) abrasion pattern at 110000 cycles. The arrow in (a) shows the sliding directions, this direction also applies to the other two figures.

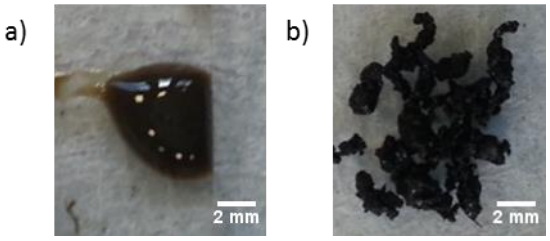

Figure 6. Collected sticky debris during the smear wear: a) NR0 collected during the test with a normal force of 4N and b) SBR50 collected during the test with a normal force of 12N.

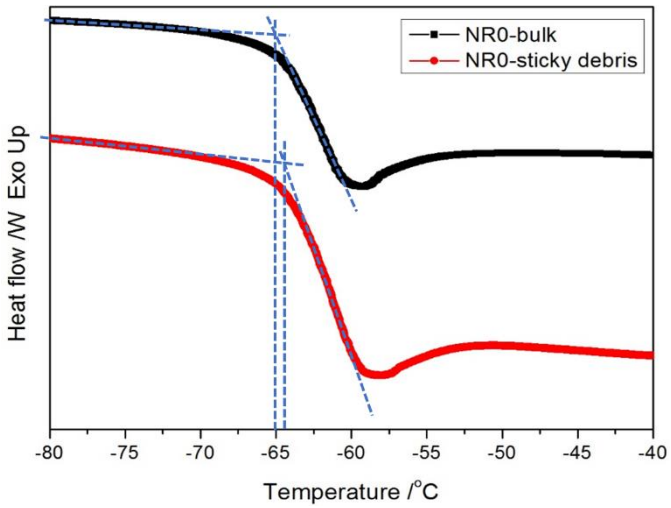

Figure 7 . DSC trace of the smear wear and bulk materials for NR0.

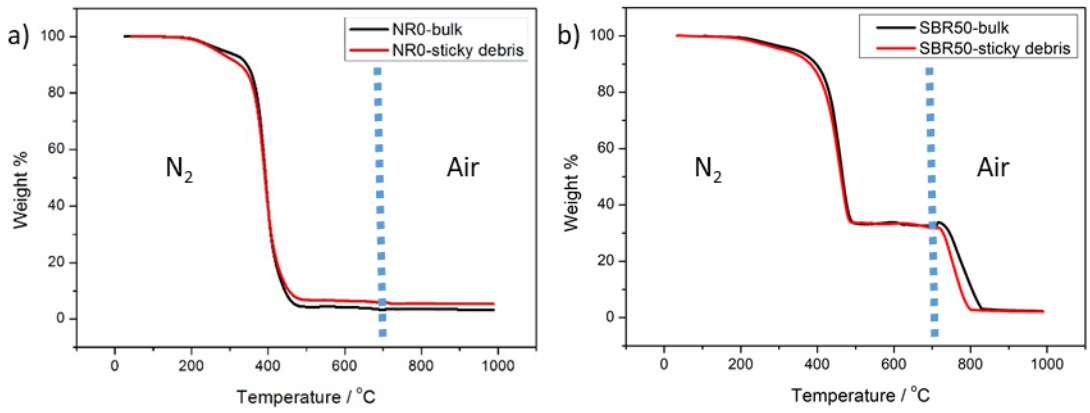

Figure 8. TGA weight loss in nitrogen up to 700 °C and in air from 700 °C to 1000 °C of a) NR0 and b) SBR50.

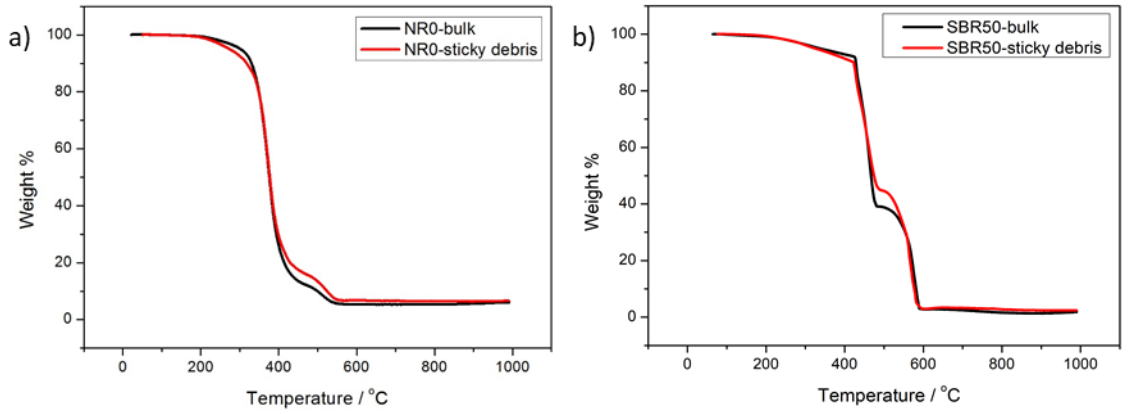

Figure 9. TGA weight loss in air of a) NR0 and b) SBR50.

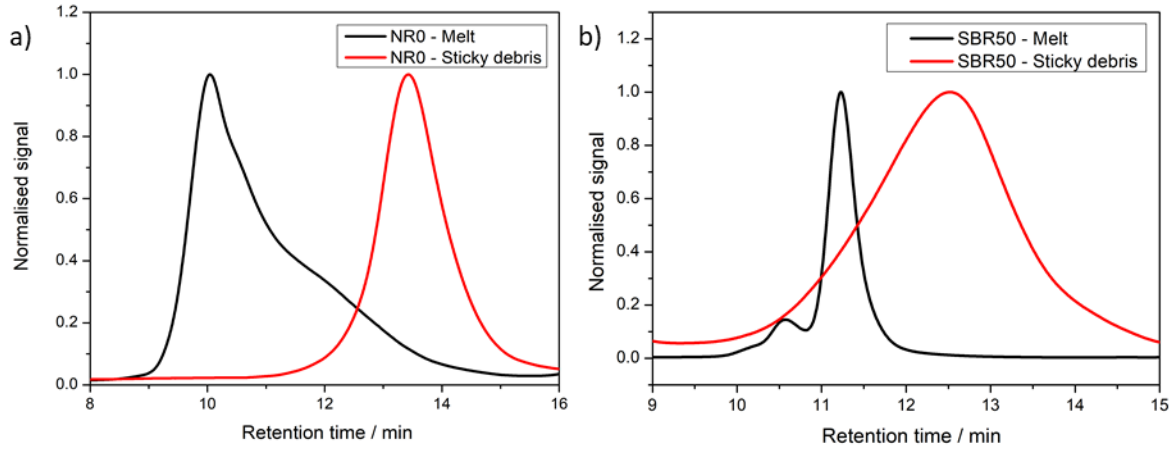

Figure 10. Normalised GPC trace of the rubber melt and smear wear of a) NR0 and b) SBR50.

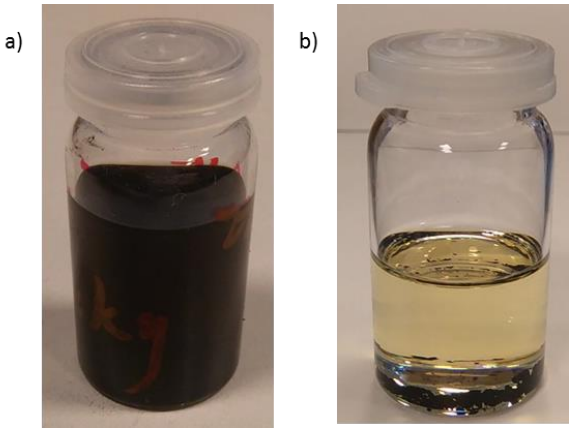

Figure 11. a) Fresh smear wear of SBR50 dissolved in toluene immediately after abrasion and b) placed in toluene after a 24 hours dwell time.

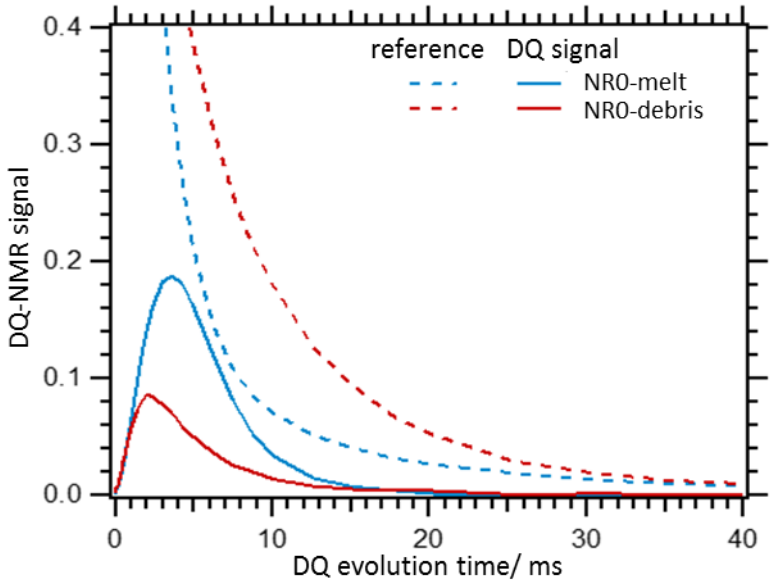

Figure 12. Reference and DQ signal (normalized to I_{ref} = 1 at zero evolution time) in uncured NR melt and NR0 sticky wear debris.

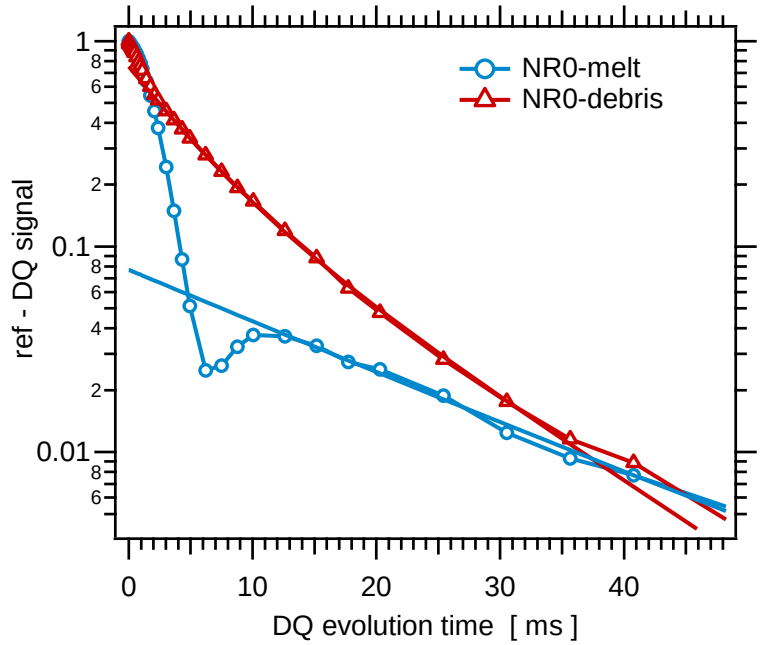

Figure 13. Reference signal subtracted DQ signal for uncured NR melt and NR0 smear wear. The long-time tail contribution is shown for each case.

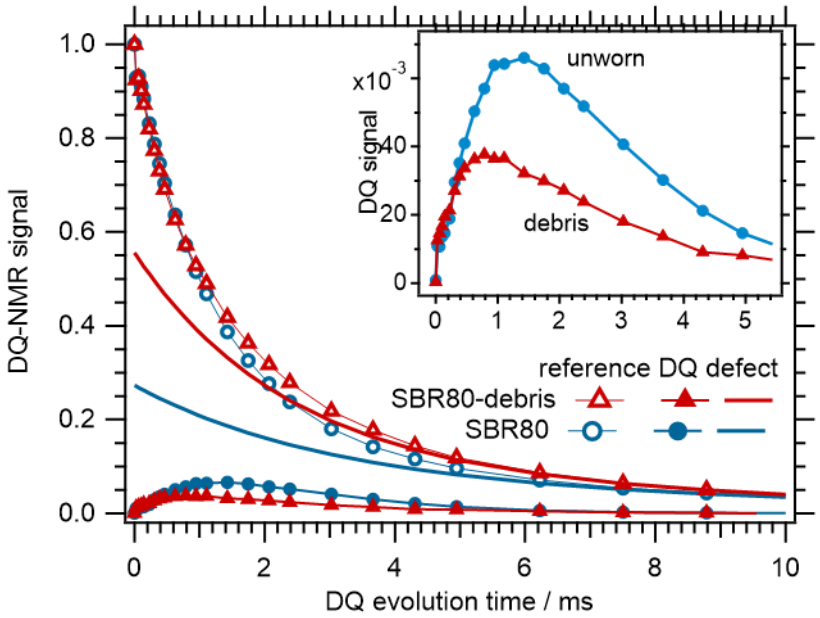

Figure 14. Reference signals and DQ signals for unworn SBR80 and SBR80 smear wear. The long-time tail contribution, corresponding to so-called defects, or uncrosslinked material, is shown for each case. Inset is a zoom of the DQ signals at short DQ evolution time.

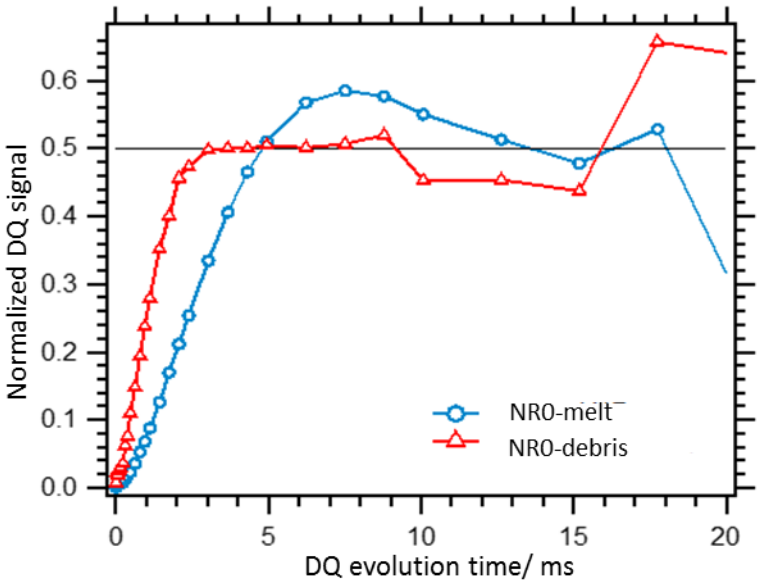

Figure 15. Normalised DQ curves for NR0 melt and NR0 smear wear.

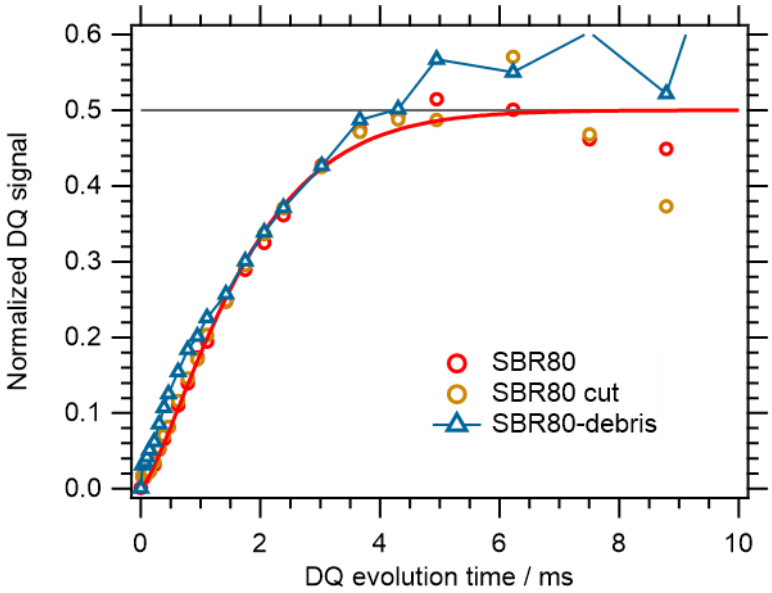

Figure 16. Normalised DQ curves for unworn SBR80, unworn SBR80 manually cut into small pieces and SBR80 smear wear debris.

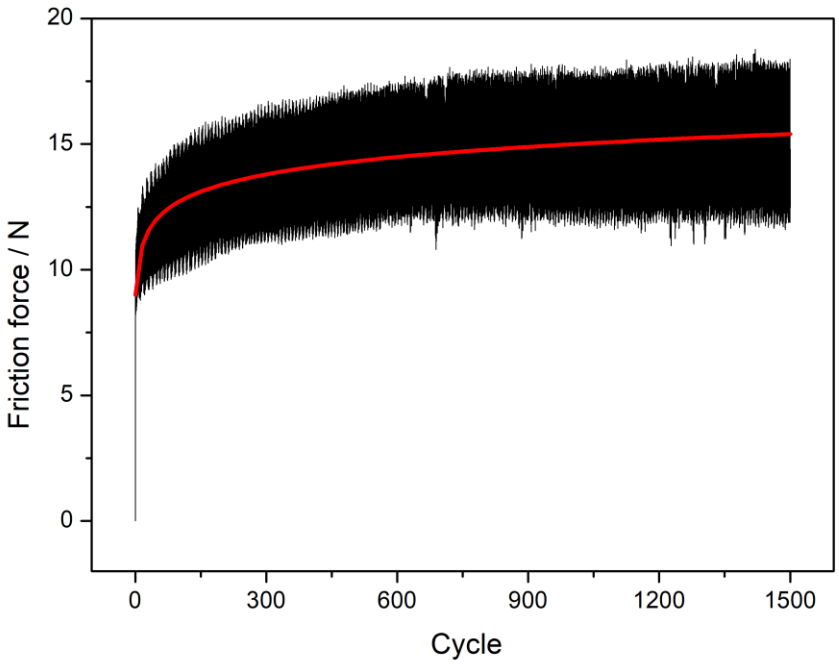

Figure 17. Friction profile during blade abrasion for SBR50 at 8 N normal force, black line: the oscillating real time recorded data and the red line: logarithmic trend of the data.

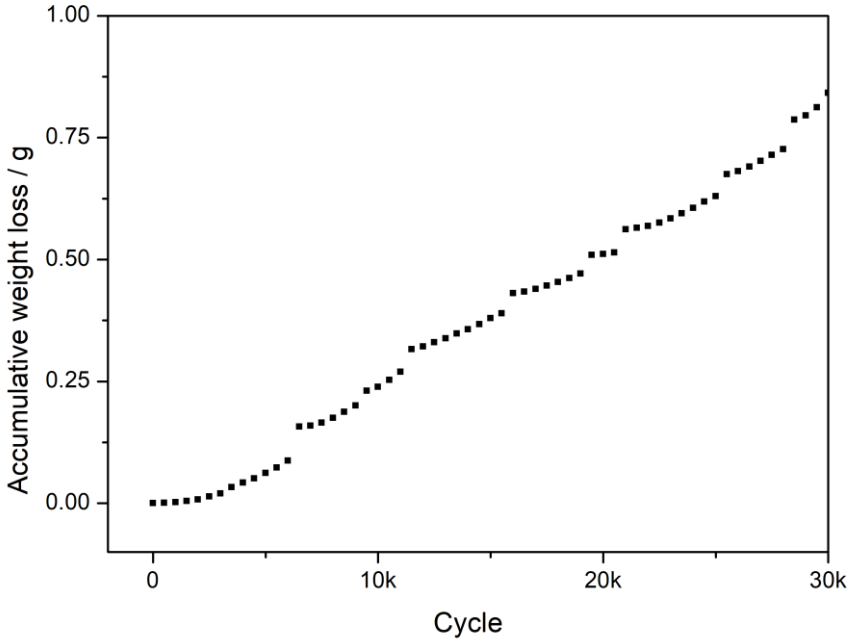

Figure 18. Abrasion loss of blade abrasion test for SBR50 under 26 N normal force.

Table 1. Formulations and curing conditions for 12.5 mm thickness rubber wheel in phr (Parts per Hundred Rubber)

Ingredient	**Trade Name**	**NR0**	**SBR50**
NR	SMR CV60	100	
SBR	BUNA VSL 4720-0HM		100
Carbon Black	N234		50
Tackifier	Koresin		3
Wax			2.5
Zinc Oxide		5	3
Stearic Acid		2	2
Antioxidant	6PPD	3	1
Accelerator	CBS	1.5	1.1
Accelerator	DPG		0.3
Sulphur		1.5	1.4
Curing Conditions			
Curing Temperature / °C		145	140
Curing Time / minutes		30	50

Table 2. Weight percent loss of thermal-oxidative degradation for NR0.

	Volatile (25 – 320 °C)	**Polymer (320 – 450 °C)**	**Char (450 – 600 °C)**	**Ash (600 – 1000 °C)**

NR0 – Bulk	8.13%	78.21%	8.21%	5.45%
NR0 - Smear wear	11.12%	71.14%	10.74%	7.00%

Table 3. Weight percent loss of thermal-oxidative degradation for SBR50.

	Volatile (25 – 420 °C)	**Polymer (420 – 500 °C)**	**Carbon Black & Char (500 – 800 °C)**	**Ash (800 – 1000 °C)**
SBR50 – Bulk	8.75%	52.12%	37.77%	1.36%
SBR50 - Smear wear	10.23%	45.02%	41.90%	2.85%

Table 4. Molecular weight of the smear wear and the uncured rubber melt.

MW averages	*Mn*	*Mw*	*PD*
NR0 melt	202011	713243	3.53
NR0 smear wear	31627	50647	1.60
SBR50 melt	380098	475832	1.25
SBR50 smear wear	64983	187082	2.88

Table 5. EDX analysis of smear wear and bulk rubbers. A carbon coating was included for NR0, so the values are normalised after carbon is removed from the analysis.

	Oxygen wt%	Sulphur wt%	Zinc wt%	Carbon wt%
NR0 - bulk	39.0	26.1	34.9	NA
NR0 - smear wear	41.7	25.1	33.2	NA
SBR50 - bulk	2.8	1.5	1.7	93.9
SBR50 - smear wear	8.5	0.7	0.4	90.4